ROYAL SOCIETY
OF CHEMISTRY

PAPER

Freely-shapable fabrication of aerogel patterns and 3D architectures by freeze-assisted transfer printing†

Wenbo Li,[ab] Jing Liu,[b] Danyang Liu,[a] Jing Li,[ab] Jiawei Wang,[b] Jiongli Li,[b] Xudong Wang,*[b] Meng Su, [ID] *[c] Chunbao Li*[d] and Yanlin Song [ID] [c]

Herein, we propose a freeze-assisted transfer printing strategy to realize freely-shapable fabrication of graphene aerogels. The competition of interfacial adhesion between the stamp and substrate was evaluated, providing the basis for controllable positioning and shaping of patterned aerogel arrays. Taking advantage of the diverse geometry building blocks, large area or complex 3D aerogel architectures can be prepared efficiently. This strategy is compatible with various concentrations of graphene inks and has no viscosity dependence, so aerogel patterns of different densities can be printed in a single pass. A gradient graphene aerogel was prepared by multilayer printing, satisfying the sensitive pressure sensing under both small deformation and large strain conditions. In addition, we have demonstrated that the strategy is applicable to abundant colloidal systems including composite nanomaterials and biopolymers. Therefore, heterogeneous aerogel structures can be realized through the principle of laminated printing using multiple materials. A bilayer aerogel with an auxetic pattern was designed, which showed magnetically controlled stretchability and stable conductivity. This demonstrates the potential application of our approach in functional device integration.

1. Introduction

Assembly of functional nanomaterials into three dimensional (3D) aerogels has attracted great interest due to their distinct high specific surface area, elasticity, porosity and ultra light-weight properties.[1–4] Low dimensional materials including graphene, carbon nanotubes and MXenes are widely used as building blocks for the construction of functional aerogels.[5–9] Their superior mechanical, thermal, and conductive performance provides a broad application prospect in energy storage, pollutant adsorption, heat insulation, electromagnetic shielding, flexible sensing, catalysis and other fields.[10–15] Graphene aerogel is a kind of macroscopic material assembled from

a AECC Beijing Institute of Aeronautical Materials, Beijing Engineering Research Centre of Graphene Application, Beijing 100095, P. R. China

b Beijing Institute of Graphene Technology, Beijing 100094, P. R. China. E-mail: netfacn@163.com

c Key Laboratory of Green Printing, Institute of Chemistry, Chinese Academy of Sciences (ICCAS), Beijing Engineering Research Center of Nanomaterials for Green Printing Technology, Beijing National Laboratory for Molecular Sciences (BNLMS), Beijing 100190, P. R. China. E-mail: sumeng1988@iccas.ac.cn

d Peoples Liberat Army Gen Hosp, Med Ctr 4, Dept Orthopaed Med, Beijing, 100853, P. R. China. E-mail: cli301@foxmail.com

† Electronic supplementary information (ESI) available. See DOI: https://doi.org/10.1039/d3tc01121f

graphene or its derivatives, with an interconnected porous network structure, which is also known as graphene foam or graphene sponge. Although the bulk form of graphene aerogel has shown functional applications in many aspects, its development from a macroscopic scale toward miniaturized patterns is of great importance for the realization of high-performance integrated devices.[16–24]

The methods for constructing graphene aerogels mainly include hydrothermal or chemical reduction,[25–27] sacrificial templates and etching process,[28–30] 3D printing techniques,[31–35] *etc.* The graphene aerogels prepared through reduction assembly and sacrifice templates are generally in simple bulk forms, which are limited by the shape of the container used in the preparation process. In addition, the hydrothermal or chemical reduction method tends to result in a large degree of volume shrinkage, so it is not easy to control the structure of graphene aerogel accurately. Moreover, due to the fragile and deformable mechanical properties of aerogel materials, they are not suitable for the subtractive manufacturing process to achieve shaping and patterning like traditional materials. Therefore, 3D printing has been utilized for the patterning of functional aerogels.[36–41]

The 3D printing approach of graphene aerogel is mainly based on micro-extrusion, which relies on a high concentration ink with high viscosity to ensure printability.[34,35,42] Although this method allows for the creation of graphene aerogels with

desired shapes, the limitation of printable inks restricts the density distribution and compositional diversity of the printed structures. In the process of printing large and complex structures, it is hard to maintain the structural integrity due to ink drying causing structural collapse and deformation. Thus, the overall processing size range is limited. Additionally, layer by layer extrusion printing is also not conducive to large-scale manufacturing in terms of processing speed and efficiency. Therefore, achieving freely-shapeable fabrication of aerogel patterns and 3D architectures remains a challenge.

In this work, we have developed a freeze-assisted transfer printing (FATP) strategy to address the shortcomings of existing approaches. Transfer printing allows high-throughput assembling of patterned aerogel arrays. Complex 3D aerogel architectures can also be achieved through multilayer printing, with the assistance of freezing that offers interfacial bonding. Through a combination of transfer printing and freezing, freely-shapeable aerogels can be efficiently prepared, which have rich material applicability and an adjustable processing size range. We demonstrate the wide adaptability of this approach to various concentrations of graphene inks and abundant colloidal materials. Moreover, we have prepared gradient graphene aerogels and heterogeneous aerogels for device integration, showing remarkable properties in pressure sensing and stretchable electronics.

2. Results and discussion

2.1. Patterning of graphene aerogel by FATP

In Fig. 1a, we propose a process flow for the fabrication of patterned graphene aerogel by FATP. First, a flexible polydimethylsiloxane (PDMS) mould with a groove pattern was prepared, which served as the printing stamp. Then, the printing ink was injected into the stamp. In this case, a dispersion of graphene oxide (GO) was taken as an example. The GO ink was frozen in the grooves of the stamp, and converted into an array of GO ice cubes. Subsequently, the filled stamp was affixed to the glass substrate at a low temperature, and left for a certain time to allow the frozen ink to bond with the glass substrate. After peeling off the stamp, the GO ice cubes were transfer printed onto the glass substrate, maintaining their patterned arrays. Followed by freeze-drying, patterned GO aerogel can be obtained. GO aerogel can further be transformed into graphene aerogel through chemical or thermal reduction, so as to achieve desirable electrical or thermal conductivities.

Fig. 1b shows the optical image of the GO aerogel array. A total of 120 aerogel units are distributed on a glass slide. Each unit has a cubic shape with a side length of 1.5 mm and a spacing of 2 mm, like an individual pixel. A resolution of 20×6 was achieved across the size range of the glass slide. The morphologies were uniform and consistent. In addition, linear and circular shaped aerogel arrays are also shown in Fig. 1c, with distributions of 20×2 and 10×3, respectively. It was observed that these tiny aerogel units undergo minimal volume shrinkage after freeze-drying. The speculated reason is that the

small volumetric aerogel units have a large specific surface; thus the ice crystals sublimate rapidly in a short period of time. In our experiment, the time for freeze-drying can be as low as 10 minutes, far less than the common durations of hours to tens of hours. These miniature aerogels can be used as basic geometric elements for the construction of graphical graphene aerogels. The typical microscopic morphology of the aerogel unit is shown in Fig. S1 (ESI†).

In the process of FATP, there exists a competition between adhesive forces among different interfaces. In order to transfer the frozen GO units from the PDMS stamp to the glass substrate, the following condition should be satisfied:

$$\gamma_{\text{ice-stamp}} < \gamma_{\text{ice-substrate}} \tag{1}$$

where $\gamma_{\text{ice-stamp}}$ represents the adhesive strength of the interface between the frozen GO and the PDMS stamp, $\gamma_{\text{ice-substrate}}$ represents the adhesive strength between the frozen GO and the glass substrate.

Disc-shaped GO ices were used to investigate the relationships between adhesive forces, where the initial density of GO was 2 mg mL^{-1}. As shown in Fig. 1d, when the diameter of the disk increases from 10 mm to 30 mm, the $\gamma_{\text{ice-stamp}}$ value decreases from 24.33 kPa to 9.85 kPa, while the $\gamma_{\text{ice-substrate}}$ value decreases from 133.25 kPa to 54.86 kPa, which is always larger than $\gamma_{\text{ice-stamp}}$. In Fig. 1e, when the thickness of the disk increases from 1 mm to 3 mm, the $\gamma_{\text{ice-stamp}}$ value increases from 10.35 kPa to 34.76 kPa, while the $\gamma_{\text{ice-substrate}}$ value has no significant change. Within the test range, eqn (1) can be satisfied. The results illustrate that it is easier to achieve the transfer printing of ice patterns with a larger diameter, or with a smaller thickness. For the GO ices of different densities, the $\gamma_{\text{ice-stamp}}$ and $\gamma_{\text{ice-substrate}}$ remained at similar values, fulfilling the conditions stated in eqn (1) (Fig. 1f). Therefore, the FATP strategy has a wider range of ink options for the printing of aerogel structures, whereas typical extrusion-based 3D printing often relies on a high concentration ink, and the inkjet-based 3D printing requires the use of low concentration ink.[32]

Glass is selected as the printing substrate, because it offers suitable adhesion strength to satisfy the competition conditions in eqn (1). Several common materials besides glass are also investigated, including Teflon, PET and PDMS. The test results are shown in Fig. S2 (ESI†). There are several advantages of using PDMS as a printing stamp. First, PDMS has low adhesion with GO ice. Second, it has an appropriate elastic modulus. Thus, the GO ice cubes can be released gradually by bending the PDMS stamp during the peeling process. Third, the light transmittance of PDMS is convenient to complete the pattern transfer at the specific position of the substrate, and also beneficial to the pattern alignment when preparing multilayer structures.

2.2. 3D fabrication of graphene aerogel by FATP

To achieve complex 3D aerogel structures, multilayer transfer printing was executed. The process flow of layered manufacturing is shown in Fig. 2a. Similar to the array pattern depicted in Fig. 1a, the first layer of frozen ink was transferred from the

This journal is © The Royal Society of Chemistry 2023

J. Mater. Chem. C, 2023, 11, 10834–10842 | 10835

Fig. 1 Patterning of graphene aerogel by FATP. (a) Schematic of the fabrication process for aerogel patterning. (b) Optical images of the cubic shaped aerogel units in a 20 × 6 array. Scale bar: 5 mm. (c) Optical images of the aerogel arrays with linear and circular shape. Scale bars: 5 mm. (d–f) The adhesive strength of $\gamma_{\text{ice-stamp}}$ and $\gamma_{\text{ice-substrate}}$ as a function of sample diameter, thickness and density.

PDMS stamp to the glass substrate. After that, additional layers of frozen ink were stacked to their previous layers step by step. Each intermediate structure was maintained for a certain time under pressure after printing, thereby enabling the layers to fit together tightly without leaving any gaps.

During the overprinting process, the substrate is changed from glass to a pre-set layer of frozen ink. Therefore, the following conditions are required to complete multilayer transfer printing:

$$\gamma_{\text{ice-stamp}} < \gamma_{\text{ice-ice}} < \gamma_{\text{ice-substrate}} \tag{2}$$

where $\gamma_{\text{ice-ice}}$ represents the adhesion strength of the interface between two frozen layers.

We investigated the $\gamma_{\text{ice-ice}}$ value using two samples of frozen GO ink with a typical disc shape, as shown in Fig. S3 (ESI†). The value of $\gamma_{\text{ice-ice}}$ is between the $\gamma_{\text{ice-stamp}}$ and $\gamma_{\text{ice-substrate}}$ values, which satisfies the equation and is feasible for transfer printing.

After the construction of the whole structure, arbitrary shaped aerogels can be obtained followed by the subsequent procedure of freeze-drying. In Fig. 2b–m, we demonstrate the ability of FATP to create complex 3D architectures through
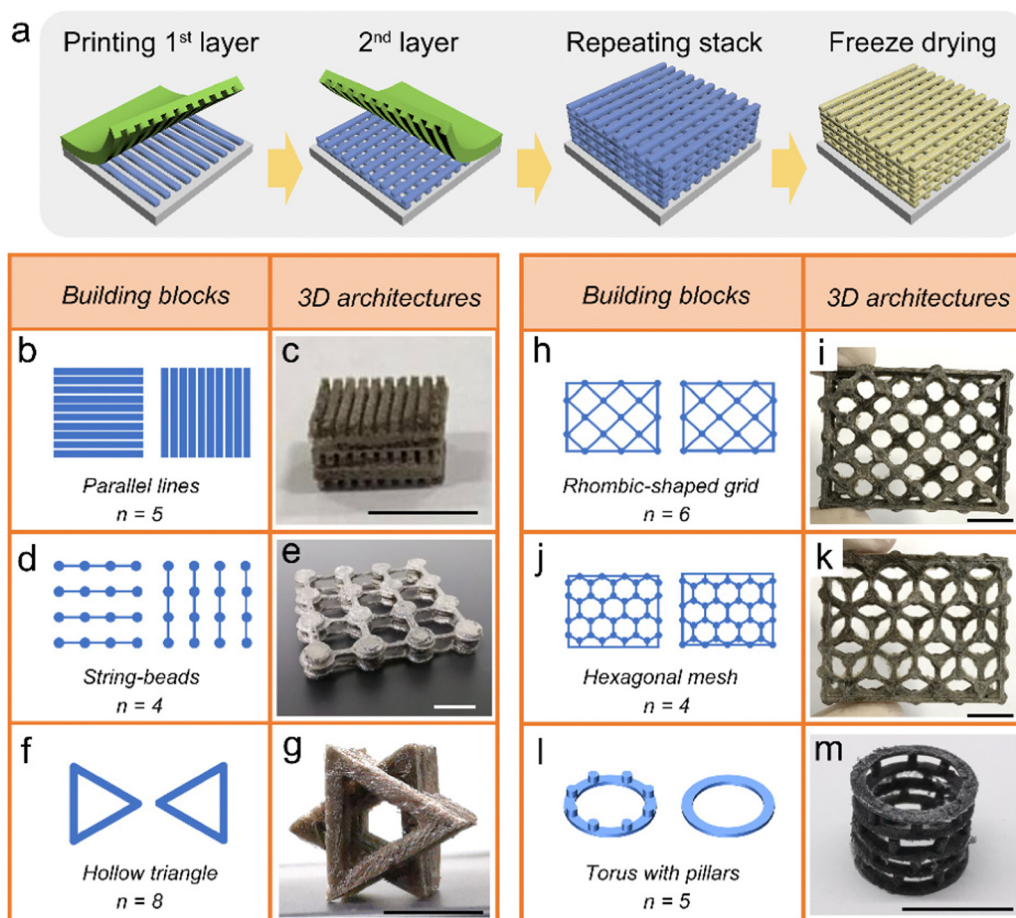
10836 | *J. Mater. Chem. C*, 2023, **11**, 10834–10842

This journal is © The Royal Society of Chemistry 2023

Fig. 2 3D fabrication of graphene aerogel by FATP. (a) Schematic diagram of the layered manufacturing process for complex aerogel architectures. (b–m) Design sketches of the building blocks and optical images of the assembled 3D architectures, in which *n* represented the number of repeating layers. The scale bars in the figures are 1 cm.

several sets of examples. In the multilayer transfer printing process, the frozen ink layers can be regarded as the building blocks. They were assembled into macroscopic 3D structures according to different geometric patterns, orientations and order of arrangement, in which *n* represented the number of repeating layers.

In the first set of examples (Fig. 2b and c), parallel linear arrays served as the building blocks and were arranged in a 90° cross pattern to form a micro-lattice structure. The orientation of interlayer arrangement can also be set at different angles by controlling the direction of transfer printing. As a special printing technique for the patterning of the aerogel structure, the processing accuracy reaches the submillimetre scale. The linear array has a width of 800 μm and an interspace of 200 μm, representing the feature size of FATP in our experiment.

As shown in Fig. 2d and e, a group of string-bead arrays was assembled. The beaded parts were connected between layers and provided a relatively strong bond. Consequently, the string parts maintained a certain span to achieve a suspended configuration. The ratio of span to width was more than 5 times, which is among the highest records in aerogel printing.

The basic design elements for FATP are not limited to filaments compared to extrusion-based 3D printing, but can

be a variety of geometric shapes. For instance, the third group consists of hollow triangles as assembly units (Fig. 2f and g), and the fourth group utilized rhombic-shaped grids as basic elements (Fig. 2h and i). Each layer regardless of its complexity can be printed in a single pass. More examples are shown in Fig. S4 (ESI†).

In addition, different asymmetric patterns can also be used as building blocks to create the overall 3D structures. In the fifth group, two different hexagonal mesh patterns were assembled into a complex structure through four layers of transfer printing. A long-span suspended configuration was formed due to the staggered arrangement of hexagonal grids (Fig. 2j and k).

We show through the last set of examples that non-planar patterns were used as building blocks for transfer printing (Fig. 2l and m). A structure containing torus shapes with pillars was directly printed, and assembled layer by layer into a spring-shaped 3D architecture. The design details are described in Fig. S5 (ESI†).

Through the above examples, we demonstrate the flexibility of FATP in constructing complex 3D structures. In particular, it can be used to construct aerogel architectures that are difficult to achieve with conventional printing methods. Moreover, this

printing approach has a long operation window, so it has advantages in the processing of large size components. Structure shrinkage or deformation caused by ink drying often occurs in the conventional printing process, but the phenomenon would be avoided in this freeze-assisted printing method.

2.3. Gradient aerogel structure by FATP

As mentioned in the previous discussion, the GO inks with various concentrations were suitable for the FATP method to prepare graphene aerogel. Furthermore, we prepared gradient graphene aerogels by arranging the GO ice cubes with different densities. An array pattern of graphene aerogels with densities of 1 to 10 mg mL^{-1} is shown in Fig. 3a. GO inks of ten concentrations were loaded into a PDMS stamp, and the gradient aerogel array was prepared through a single pass of transfer printing. As shown in Fig. 3b and c, each density of GO ice cubes was taken as a separate layer, and the 3D structure of density-gradient aerogel was prepared by stacking. It shows obvious difference of brightness and shade in these layers, both in the frozen (Fig. 3b) and dry (Fig. 3c) states. Fig. 3d shows the SEM images of graphene aerogel, with densities of 2, 4, 6, and 8 mg mL^{-1}. The GO sheets assembled into cellular networks with different porosities, which follows the mechanism of ice-templating.

To demonstrate the performance advantages of gradient aerogel, a gradient 4-layer structure was prepared through a multiple printing process. The initial density of each layer was 8, 6, 4, and 2 mg mL^{-1}, in the descending order of superposition. After freeze drying and chemical reduction, the gradient graphene aerogel was filled with PDMS, and turned into a conducting elastomer. This conducting elastomer was applied in pressure sensors, as shown in Fig. 3e. For a comparative test, pressure sensors having homogeneous structures were also prepared. Each device was printed individually using a single concentration ink, with the process repeated four times. From the results shown in Fig. 3f and g, the response characteristics of pressure sensors with homogeneous structures varies with their initial concentrations, but there is no obvious regularity. Under the condition of small strain (0.2–1.0%), the response change rate of pressure sensor with an initial concentration of 4 mg mL^{-1} is higher than that of the other homogeneous sensors, while the sensor with a concentration of 2 mg mL^{-1} has a relatively minimal performance. In the range of large strain (10–30%), the 2 mg mL^{-1} sensor presents a higher response change rate, while the 8 mg mL^{-1} sensor has a lower performance. However, in both test ranges, the pressure sensor with a gradient structure shows the most superior response characteristics, which proves that the gradient sensor can meet
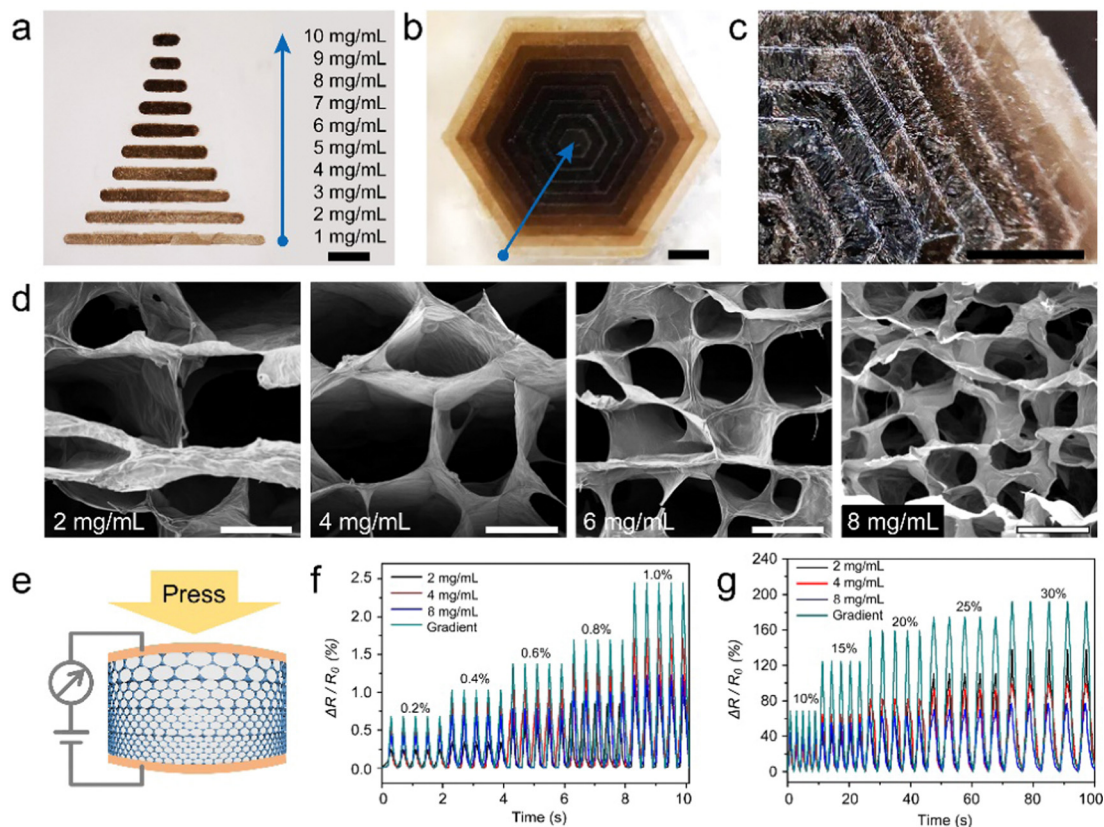

Fig. 3 Gradient aerogel structure by FATP. (a) Patterning of gradient aerogel through a single pass of transfer printing. (b and c) Multilayer transfer printed gradient aerogel in the frozen and dry states. (d) SEM images showing the typical morphology of graphene aerogel with different densities. (e) Schematic showing the conductive elastomer made from gradient aerogel for pressure sensing. (f and g) Resistance change rates of the pressure sensors with homogeneous and gradient structures under small deformation and large strain. Scale bars: 1 cm (a–c); 50 μm (d).

10838 | *J. Mater. Chem. C*, 2023, **11**, 10834–10842

This journal is © The Royal Society of Chemistry 2023

the requirements under both small deformation and large strain conditions. Therefore, the gradient aerogels achieved through rational structural design have great potential for application.

2.4. Multi-material integration by FATP

Taking graphene-based materials as an example, we have demonstrated that FATP can be used as an effective method to prepare aerogel patterns or complex 3D structures. The method is also suitable for various systems of colloidal materials, including polymer solutions, low-dimensional nanomaterials, and their composites. Fig. 4a respectively shows the aerogel patterns prepared using GO, sodium alginate, bacterial cellulose, silver nanowires and GO/Fe$_3$O$_4$. The common feature of these materials is that they can be assembled through an ice-templating mechanism to form a porous 3D morphology. Aerogels of each material start from functional inks consisting of various components, and can further be patterned through the FATP approach. Combined with specific shape and structure design, these aerogels provide a rich material basis for the fabrication of functional devices, which will promote their application in lithium-ion batteries, catalysis, sensors, solar distillation, electric heating and other fields.

According to the principle of laminated manufacturing, heterogeneous aerogels were produced through FATP using multiple materials. The integration of multiple materials was realized on different layers or even in different areas of the same layer. The heterogeneous aerogel structures of tai-chi, panda, petal and other patterns are presented in Fig. 4b and Fig. S6 (ESI†). Sodium alginate and GO were used for sample preparation, corresponding to the white area and the dark area. The two components were first connected in the frozen state by the interaction of ices. Then, the GO sheets and sodium alginate molecules were self-assembled through the mechanism of freeze-drying, and bonded together at the interface. Additionally, we printed an integrated structure using four types of materials. Three groups of heterogeneous interfaces were formed between the adjacent layers, as shown in Fig. S7 (ESI†).

Through the integration of heterogeneous materials, we designed a stretchable aerogel device that can be operated by magnetic field (Fig. 4c). The device includes a conductive layer and a magnetic layer. The conductive layer consists of a graphene aerogel with an auxetic structure, and the magnetic layer was made using a nanocomposite aerogel of GO/Fe$_3$O$_4$. The interface between the two layers can clearly be seen from the SEM image. Aerogel materials generally show compression
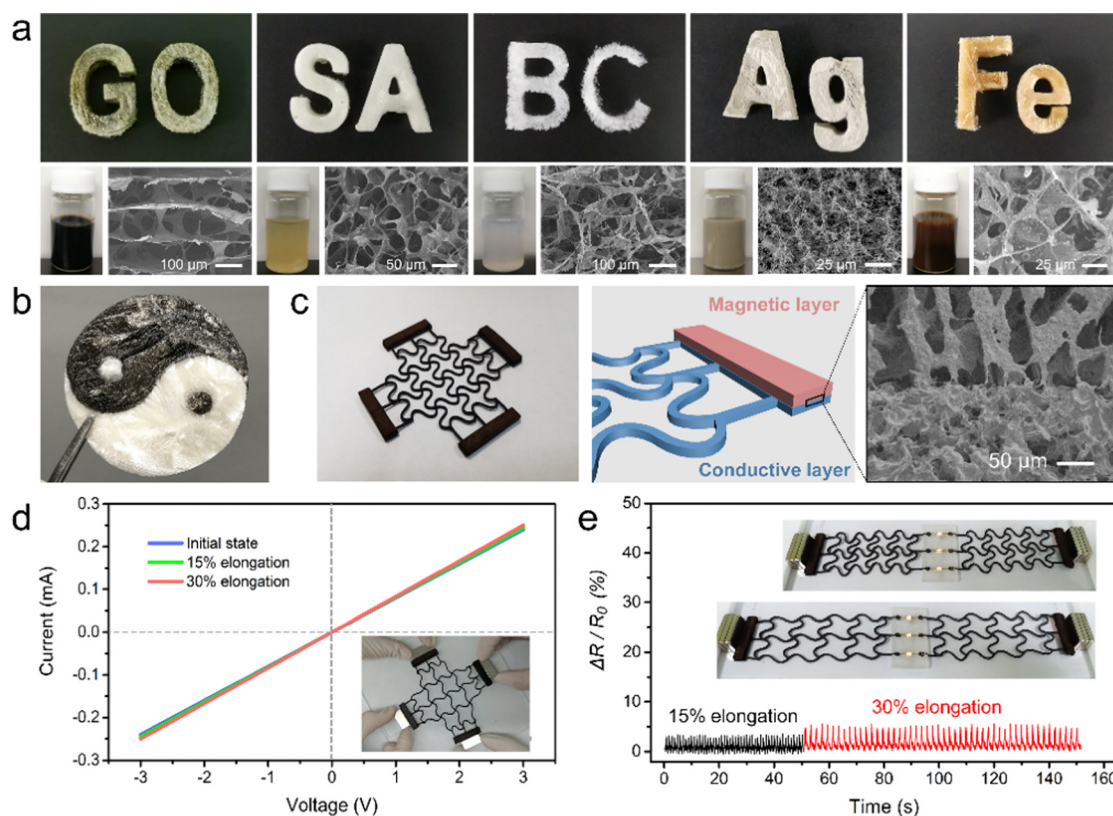

Fig. 4 Multi materials integration by FATP. (a) Various colloidal systems are suitable for the FATP approach, including GO, sodium alginate, bacterial cellulose, silver nanowires and GO/Fe$_3$O$_4$ nanocomposites. The images respectively show the corresponding inks and the morphology of aerogels. (b) A heterogeneous aerogel structure with a tai-chi pattern by integration of GO and sodium alginate. (c) A heterogeneous aerogel device with an auxetic pattern by integration of a conductive layer and a magnetic layer. (d) The current–voltage curves of the aerogel device under initial state and elongation. The inset photograph shows the stretchability of the device that is operated using magnets. (e) The aerogel device as a lightweight conductor showing small fluctuations in rates of resistance change during cyclic stretching. The inset photographs demonstrate the shape change of the auxetic pattern.

This journal is © The Royal Society of Chemistry 2023

J. Mater. Chem. C, 2023, **11**, 10834–10842 | **10839**

properties, but without the ability to stretch. While in this case, the auxetic pattern design and the porous nature of the aerogel synergistically counteracts the tensile stress, which enables the device to be stretchable. Attributed to the lightweight property of aerogel materials, magnetic field is sufficient to drive the device for controllable deformation. We conducted a test on this patterned aerogel, and found that the device can maintain good stability under large strain (Fig. 4d). In the strain range of 15% or 30%, the overall change rate of electrical conductivity is less than 5%. It is further used as a lightweight conductor, as shown in Fig. 4e. Two sets of the designed aerogel electrodes were connected with LEDs, and loaded on the stepping motor system for cyclic tensile experiment. The detailed construction for the stretchable device is shown in Fig. S8 (ESI†). When the elongation was controlled as 15% or 30%, the electrical signals of the conducting aerogel electrodes showed very uniform and small fluctuations over at least 20 continuous cycles. Along with the movement of the magnet on the stepping motor, the auxetic patterned aerogel electrodes can stably expand and shrink at a speed of 50 mm s^{-1}. The LEDs maintained consistent brightness during the stretching process (Movie S1, ESI†). This lightweight, stretchable, magnetically controlled aerogel electrode can be used in flexible electronics, micro-robotics and other fields for potential applications.

3. Conclusions

We have demonstrated that FATP is an efficient strategy to assemble aerogel materials into miniature patterns and 3D structures. In contrast to extrusion-based 3D printing, the inks used in this method are viscosity independent, making it applicable to a wide range of materials. Gradient graphene aerogels are prepared with inks of various concentrations. The results show that gradient aerogels show more sensitive pressure-response properties than homogeneous aerogels. It provides enlightenment for the future development of aerogels with composition or structural gradient to explore novel applications. In addition, heterogeneous aerogels can be achieved by printing multiple materials. We have prepared a lightweight, stretchable, magnetically controlled aerogel electrode. The porous characteristics and auxetic configurations of the aerogel enable it to maintain stable conductivity, making it suitable for application in stretchable electronics. The 3D electrodes designed through this approach can also find opportunities in the research fields such as micro batteries and catalytic platforms. Moreover, the FATP method benefits from the advantages of the long operation window, high-throughput printing of building blocks in a single pass, and availability for the long-span suspended structures. Therefore, it can act as an effective alternative or an important supplement to extrusion-based 3D printing, which will inspire the exploration of aerogels with expanded functions.

4. Experimental section

4.1. Materials and ink preparation

The GO sheets were synthesized according to our previous research.[21] Sodium alginate and Fe_3O_4 nanoparticles were purchased from Shanghai Aladdin Biochemical Technology Co., Ltd. Bacterial cellulose was purchased from Guilin Qihong Technology Co. Ltd. Silver nanowires were obtained from Qingdao Nanoprinting Technology Co., Ltd. Graphene flakes were obtained from Deyang Carbonene Technology Co., Ltd. The above materials were uniformly dissolved or dispersed in water to yield the aqueous inks.

4.2. Fabrication of printing stamps

The printing stamps were fabricated through a replica moulding method. First, the target pattern or structure was printed using a stereolithography 3D printer (FormLabs, Form2); thereby a resin mould with an embossed pattern was obtained. Subsequently, the 3D printed resin mould was replicated using PDMS (Dow Corning, Sylgard 184). The PDMS was cured at 80 °C for 3 h. After peeling from the 3D printed resin mould, a soft mould with groove patterns was formed. It was used as the printing stamp for ink filling and transfer printing of aerogels.

4.3. Process of transfer printing

The inks were filled into the grooves of the printing stamps using an air-powered fluid dispenser (EFD, Ultimus I). Then the filled stamps were kept in a cryogenic refrigerator at −80 °C. The freezing time depends on the size of the patterns. After that the printing stamps were attached to the glass substrate under pressure or through wetting with a trace amount of water. The operation was executed with the assistance of a semiconductor chilling plate. Finally, the PDMS stamp was peeled off to leave the frozen ink onto the glass substrate. The transfer printing process was completed.

4.4. Fabrication of pressure sensors and stretching devices

The pressure sensors with gradient structure and homogeneous structure were both fabricated by repeating four layers of printing process. Each layer was cake-shaped, with a diameter of 15 mm and a height of 1.5 mm. The chemical reduction of GO aerogel was conducted by fumigation with hydrazine hydrate at 95 °C for 3 h. Pressure sensors were then encapsulated with PDMS and connected to copper electrodes with conductive silver glue for subsequent tests.

The stretching device was fabricated by using two types of inks. The ink for the conducting layer was prepared by dispersion of graphene flakes in 2 wt% sodium alginate solution, in which the concentration of graphene flake was 10 mg mL^{-1}. The ink for the magnetic layer was based on GO/Fe_3O_4 nanocomposites, with concentrations of 8 mg mL^{-1} and 20 mg mL^{-1}, respectively.

4.5. Characterization of structures and properties

The SEM images were acquired on a Phenom Nano proX system. The adhesion data were recorded using a gauge meter (0–100 N, WD-100) attached with a displacement platform (EFD, EV4). The digital source meter (Keithley 2450) equipped with an electromechanical testing system (Suns Technology, UTM6103) was used to measure the electrical signals under pressure and tension.

10840 | *J. Mater. Chem. C*, 2023, **11**, 10834–10842

This journal is © The Royal Society of Chemistry 2023

Author contributions

Wenbo Li and Meng Su put forward the methodology and carried out the writing. Jing Liu, Danyang Liu, Jing Li and Jiawei Wang carried out the investigation, data curation and validation. Jiongli Li and Xudong Wang carried out the project administration, Chunbao Li and Yanlin Song carried out the supervision and formal analysis.

Conflicts of interest

There are no conflicts to declare.

Acknowledgements

References

1 S. Zhao, G. Siqueira, S. Drdova, D. Norris, C. Ubert, A. Bonnin, S. Galmarini, M. Ganobjak, Z. Pan, S. Brunner, G. Nystrom, J. Wang, M. M. Koebel and W. J. Malfait, *Nature*, 2020, **584**, 387–392.

2 H. Joukhdar, A. Seifert, T. Jungst, J. Groll, M. S. Lord and J. Rnjak-Kovacina, *Adv. Mater.*, 2021, **33**, 2100091.

3 M. Li, X. Dai, W. Gao and H. Bai, *Acc. Mater. Res.*, 2022, **3**, 1173–1185.

4 L. Qiu, J. Z. Liu, S. L. Chang, Y. Wu and D. Li, *Nat. Commun.*, 2012, **3**, 1241.

5 X. Cao, J. Zhang, S. Chen, R. J. Varley and K. Pan, *Adv. Funct. Mater.*, 2020, **30**, 2003618.

6 X. Huang, J. Huang, D. Yang and P. Wu, *Adv. Sci.*, 2021, **8**, 2101664.

7 L. Lv, P. Zhang, H. Cheng, Y. Zhao, Z. Zhang, G. Shi and L. Qu, *Small*, 2016, **12**, 3229–3234.

8 D. Xu, S. Yang, P. Chen, Q. Yu, X. Xiong and J. Wang, *Carbon*, 2019, **146**, 301–312.

9 J. Yang, Y. Li, Y. Zheng, Y. Xu, Z. Zheng, X. Chen and W. Liu, *Small*, 2019, **15**, 1902826.

10 Y. Pang, H. Tian, L. Tao, Y. Li, X. Wang, N. Deng, Y. Yang and T. Ren, *ACS Appl. Mater. Interfaces*, 2016, **8**, 26458–26462.

11 K. Fu, Y. Wang, C. Yan, Y. Yao, Y. Chen, J. Dai, S. Lacey, Y. Wang, J. Wan, T. Li, Z. Wang, Y. Xu and L. Hu, *Adv. Mater.*, 2016, **28**, 2587–2594.

12 C. Zhang, K. Shen, B. Li, S. Li and S. Yang, *J. Mater. Chem. A*, 2018, **6**, 19960–19966.

13 K. Zhang, X. Jiao, L. Zhou, J. Wang, C. Wang, Y. Qin and Y. Wen, *Biomaterials*, 2021, **276**, 121040.

14 T. Xue, Z. Huang, P. Zhang, M. Su, X. Hu, T. Wu, B. Fan, G. Chen, G. Yu, W. Liu, X. Liu, Y. Zhang and Y. Song, *InfoMat*, 2022, **4**, e12358.

15 C. Huang, J. Peng, S. Wan, Y. Du, S. Dou, H. D. Wagner, A. P. Tomsia, L. Jiang and Q. Cheng, *Angew. Chem., Int. Ed.*, 2019, **58**, 7636–7640.

16 P. Xiao, S. Du, T. Zhang, N. Qiu, J. Zhang, Y. Huang, C. Wan, R. Jordan, Q. Huang, Z. Liu and T. Chen, *Adv. Mater. Interfaces*, 2017, **4**, 1600867.

17 T. Xue, H. Yang, B. Shen, F. Li, M. Su, X. Hu, W. Liu and Y. Song, *J. Mater. Chem. C*, 2019, **7**, 6317–6322.

18 L. Liu, Y. Huang, F. Li, Y. Ma, W. Li, M. Su, X. Qian, W. Ren, K. Tang and Y. Song, *Chem. Commun.*, 2018, **54**, 4810–4813.

19 B. An, Y. Ma, W. Li, M. Su, F. Li and Y. Song, *Chem. Commun.*, 2016, **52**, 10948–10951.

20 W. Li, Y. Li, M. Su, B. An, J. Liu, D. Su, L. Li, F. Li and Y. Song, *J. Mater. Chem. A*, 2017, **5**, 16281–16288.

21 W. Li, F. Li, H. Li, M. Su, M. Gao, Y. Li, D. Su, X. Zhang and Y. Song, *ACS Appl. Mater. Interfaces*, 2016, **8**, 12369–12376.

22 K. Pang, X. Song, Z. Xu, X. Liu, Y. Liu, L. Zhong, Y. Peng, J. Wang, J. Zhou, F. Meng, J. Wang and C. Gao, *Sci. Adv.*, 2020, **6**, eabd4045.

23 M. Zhang, R. Guo, K. Chen, Y. Wang, J. Niu, Y. Guo, Y. Zhang, Z. Yin, K. Xia, B. Zhou, H. Wang, W. He, J. Liu, M. Sitti and Y. Zhang, *Proc. Natl. Acad. Sci. U. S. A.*, 2020, **117**, 14667–14675.

24 Q. Zhang, X. Xu, D. Lin, W. Chen, G. Xiong, Y. Yu, T. S. Fisher and H. Li, *Adv. Mater.*, 2016, **28**, 2229–2237.

25 C. Li, D. Jiang, H. Liang, B. Huo, C. Liu, W. Yang and J. Liu, *Adv. Funct. Mater.*, 2018, **28**, 1704674.

26 H. Yang, Z. Li, G. Sun, X. Jin, B. Lu, P. Zhang, T. Lin and L. Qu, *Adv. Funct. Mater.*, 2019, **29**, 1901917.

27 C. Li, Z. Yang, Z. Tang, B. Guo, M. Tian and L. Zhang, *Chem. Eng. J.*, 2019, **363**, 300–308.

28 J. Chen, K. Sheng, P. Luo, C. Li and G. Shi, *Adv. Mater.*, 2012, **24**, 4569–4573.

29 X. Xu, J. Du, Q. Cao, D. Zhang, C. Li, G. Fu, Y. Gao, J. Yang, C. Guan and W. Huang, *Adv. Funct. Mater.*, 2023, **33**, 2300904.

30 B. G. Choi, M. Yang, W. H. Hong, J. W. Choi and Y. S. Huh, *ACS Nano*, 2012, **6**, 4020–4028.

31 Y. Jiang, Z. Xu, T. Huang, Y. Liu, F. Guo, J. Xi, W. Gao and C. Gao, *Adv. Funct. Mater.*, 2018, **28**, 1707024.

32 Q. Zhang, F. Zhang, S. P. Medarametla, H. Li, C. Zhou and D. Lin, *Small*, 2016, **12**, 1702–1708.

33 J. Du, G. Fu, X. Xu, A. M. Elshahawy and C. Guan, *Small*, 2023, 2207833.

34 C. Zhu, T. Y. Han, E. B. Duoss, A. M. Golobic, J. D. Kuntz, C. M. Spadaccini and M. A. Worsley, *Nat. Commun.*, 2015, **6**, 6962.

35 E. Garcia-Tunon, S. Barg, J. Franco, R. Bell, S. Eslava, E. D'Elia, R. C. Maher, F. Guitian and E. Saiz, *Adv. Mater.*, 2015, **27**, 1688–1693.

36 J. Yan, G. Zhi, D. Kong, H. Wang, T. Xu, J. Zang, W. Shen, J. Xu, Y. Shi, S. Dai, X. Li and Y. Wang, *J. Mater. Chem. A*, 2020, **8**, 19843–19854.

This journal is © The Royal Society of Chemistry 2023

J. Mater. Chem. C, 2023, **11**, 10834–10842 | **10841**

37 K. Cao, M. Wu, J. Bai, Z. Wen, J. Zhang, T. Wang, M. Peng, T. Liu, Z. Jia, Z. Liang and L. Jiang, *Adv. Funct. Mater.*, 2022, **32**, 2202360.

38 L. Li, Z. Deng, M. Chen, Z. Z. Yu, T. P. Russell and H. B. Zhang, *Nano Lett.*, 2023, **23**, 155–162.

39 Q. Cheng, Z. Sheng, Y. Wang, J. Lyu and X. Zhang, *ACS Nano*, 2022, **16**, 4905–4916.

40 S. Jambhulkar, S. Liu, P. Vala, W. Xu, D. Ravichandran, Y. Zhu, K. Bi, Q. Nian, X. Chen and K. Song, *ACS Nano*, 2021, **15**, 12057–12068.

41 J. Feng, B. L. Su, H. Xia, S. Zhao, C. Gao, L. Wang, O. Ogbeide, J. Feng and T. Hasan, *Chem. Soc. Rev.*, 2021, **50**, 3842–3888.

42 F. Wang, Y. Jiang, Y. Liu, F. Guo, W. Fang, Z. Xu and C. Gao, *Carbon*, 2020, **159**, 166–174.